

EXPERIMENTAL RESEARCH ON HELICOPTER TAIL SHAKE PHENOMENON

Iskandar Shah Ishak*, Shuhaimi Mansor, Tholudin Mat Lazim

Department of Aeronautical Engineering,
Faculty of Mechanical Engineering,
Universiti Teknologi Malaysia,
81310 UTM Skudai,
Johor, Malaysia

ABSTRACT

Helicopter tail shake phenomenon is still remained as a long dragged issue that adversely affected the overall performance, occupants' comfort and handling qualities of helicopter. The objective of this research is to improve basic understanding of the viscous unsteady flow phenomenon observed behind the helicopter tail part. For this, a wind tunnel test had been conducted with a rigid 14% generic model of Eurocopter 350Z helicopter in the Universiti Teknologi Malaysia- Low Speed Tunnel (UTM-LST) with a test section size of 2m x 1.5m x 5.8m and 288 km/hr maximum test wind speed. The model, supplied by Eurocopter France, is equipped with a motor that can rotate the main rotor up to 900 rpm during wind-on condition. As the induced wake, which consequently causing tail to shake, differs with angle of attack and yaw angle, the wind tunnel test was performed in a range angle of -10° to $+10^\circ$, respectively. The selected test wind speed was 40 m/s, which corresponds to a Reynolds number of 3.7×10^6 . To investigate the characteristics of the induced wake, velocity fluctuation mapping using hotwire was done at 3 different planes behind the model with each plane consists of 4 measurement points. Results obtained later depict some interesting facts of this wake phenomenon.

Keywords: *Helicopter tail shake phenomenon, unsteady flow, wake analysis*

1.0 INTRODUCTION

This present research aims to improve basic understanding on unsteady aerodynamic wake that contribute to helicopter tail shake phenomenon. It is a challenging issue to understand as it involves an interaction between aerodynamic flow excitation, which related to flight parameters & structural response, which related to structure characteristics. A good understanding of this matter is necessary as a typical aspect of tail shake that it has unsteady random character, indicating that the wake induced excitation is in also unsteady of nature [1].

The tail shake is partly due to the unsteady flow contributed from the main rotor assembly that hit the vertical tail which consequently causing the tail shake

* Corresponding author: E-mail: shah@fkm.utm.my

phenomenon as shown in Figure 1. This shaking tail, besides influencing helicopter performance, will transmit vibrations to the cockpit and somehow will deteriorate the level of comfort, as well adversely affect the crew efficiency as illustrated in Figure 2. Interactional Aerodynamic (I/A) remains, despite a considerable effort made by different companies over the last two decades [1], difficult to predict with confidence before the first flight of a new helicopter. General complexity of modern, compact helicopter design, associated with scaling difficulties, are contributing factors towards limited success in predicting I/A related vibration problems.

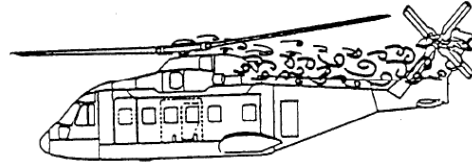


Figure 1: Schematic of tail shake phenomenon [1]

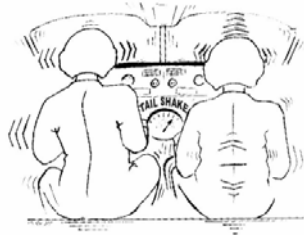


Figure 2: Comfort deteriorating [1]

2.0 TEST DESCRIPTION

The tests were conducted at the Universiti Teknologi Malaysia-Low Speed Tunnel (UTM-LST) with a test section size of 2m x 1.5m x 5.8m and 288km/hr maximum test wind speed. For this experimental investigation, the wind tunnel speed was set at 40 m/s, which corresponds to a Reynolds number of 3.7×10^6 . A generic model of 350Z Eurocopter helicopter, with a scaled down factor of 14% was used. The model with a length of 1.45m, was supplied by Eurocopter France. It is equipped with only main motor i.e. no tail motor, and not dynamically scaled i.e. any structural response of the model is not representing the actual structural response of the real 350Z helicopter.

To determine the wake characteristics which leads to tail shake, a mapping process using a hotwire was done at 3 different planes behind the model with each plane consists of 4 measurement points, respectively. Figure 3 shows schematic diagram of the experimental set-up.

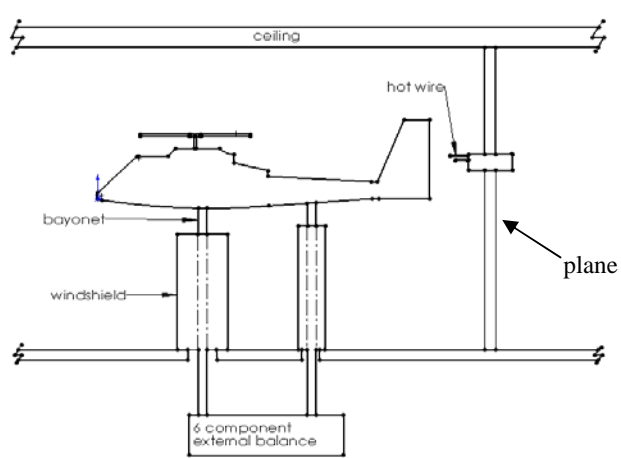


Figure 3: Schematic diagram of experimental set-up

The location of the planes are as follows:

- i) Plane A (300 mm behind the end of tail part)
- ii) Plane B (200 mm behind the end of tail part)
- iii) Plane C (100 mm behind the end of tail part)

For each plane, the hotwire were located at 4 different positions:

- i) Point 1 ($z = 1120$ mm, $x = \text{Plane A@B@C}$, $y = 0$)
- ii) Point 2 ($z = 965$ mm, $x = \text{Plane A@B@C}$, $y = 0$)
- iii) Point 3 ($z = 965$ mm, $x = \text{Plane A@B@C}$, $y = 250$ mm)
- iv) Point 4 ($z = 1120$ mm, $x = \text{Plane A@B@C}$, $y = 250$ mm)

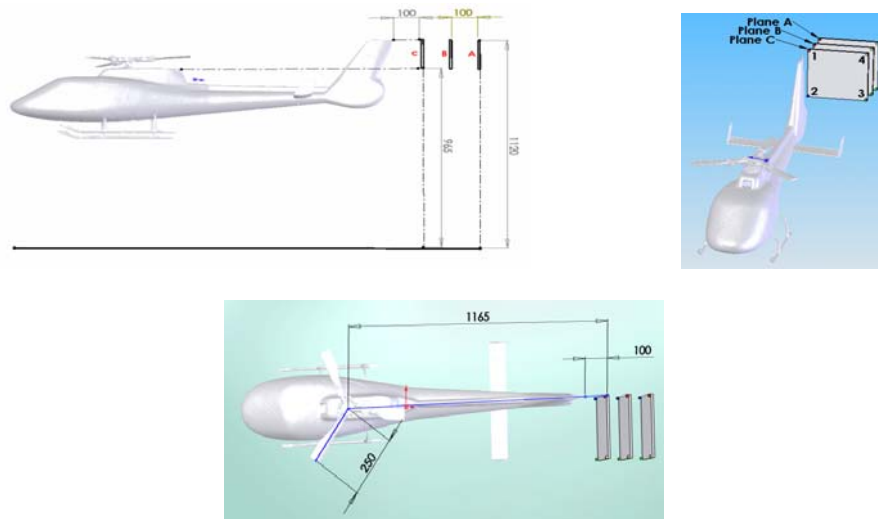


Figure 4: Turbulence mapping coordinates (All dimension in mm)

Figure 4 indicates the turbulence mapping coordinates used. The z direction is in the vertical axes. The distance shown is taken from the test section floor. The y direction is in lateral axes. The distance shown is taken from centre of test section to left side.

DANTEC single hotwire type 55P01, as shown in Figure 5, was used for determining velocity fluctuations at each point respectively. Altogether 2 hotwires from this type had been used throughout all the tests.



Figure 5: Single hotwire type 55P01

The turbulence intensity is defined by [2]:

$$\text{Turbulence Intensity: } T_u = \frac{U_{rms}}{U_{mean}}$$

The velocities are defined by the following equations and illustrated in Figure 6.

Standard deviation of velocity, U_{rms} :

$$U_{rms} = \left[\frac{1}{N-1} \sum_1^N (U_i - U_{mean})^2 \right]^{0.5}$$

Mean velocity, U_{mean} :

$$U_{mean} = \frac{1}{N} \sum_1^N U_i$$

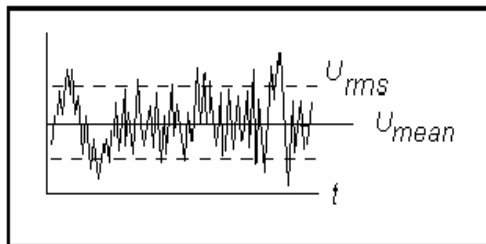


Figure 6: Schematic graph of U_{rms} and U_{mean} [2]

Prior to the tests, each wire has individually undergone velocity calibration process. This is due to fact that each wire has its own characteristics, which has different calibration slope. Figure 7 shows the hotwire for the calibration process.



Figure 7: Hotwire during velocity calibration process

In principle, both wires should give the same results for the same point location in an effort. To confirm this, experiments had been conducted for several random points and the result agree with each other. In addition, two hot wire set-up files had been initialised for results comparison as shown in Table 1.

Table 1: Hotwire set-up files

	Set-up 1	Set-up 2
Sampling Frequency (Hz)	600	25 000
Number of samples	32 768	150 000

Table 2: Turbulence intensity at plane C for $V = 50 \text{ ms}^{-1}$ and main rotor rpm = 300

Point	Turbulence Intensity (%)	
	Set-up 1	Set-up 1
2	11.484	11.420
4	0.242	0.231

Table 2 shows the results obtained. It may be concluded that for static results, the sampling frequency and number of samples has a minimal influence on the static average data. Even though the blade could be assumed as not the source of wake excitation for tail shake [3], test was still needed to be conducted for short blade, which is only at one-third of original blade length (0.25m in radius). This is because without blade, the physical end of sleeve tip would become different which consequently influence the wake characteristics. Figure 8 and Figure 9 indicates the short blade model and the hub assembly of the main rotor respectively.

To determine the test wind speed, Reynolds sweep had been conducted from 10 m/s to 40 m/s at zero angle of attack and yaw angles for model. Figure 10 displays result for Point 2, Plane B.



Figure 8: Model with short blade



Figure 9: Main rotor hub assembly

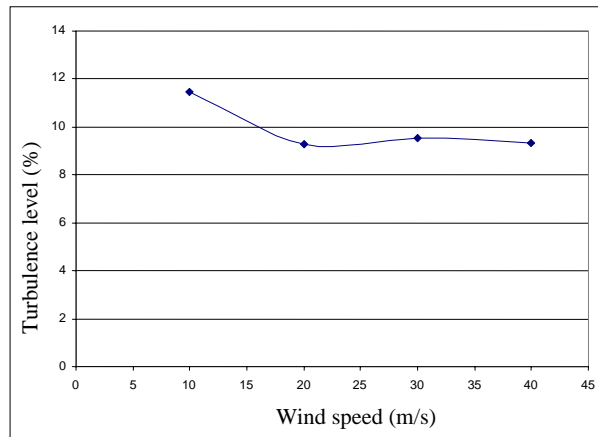


Figure 10: Turbulence intensity at Reynolds sweep with main rotor at 900 rpm

Graph in Figure 10 shows that at velocity above 20 m/s, the turbulence intensity, at this specific location, become almost independent of free stream velocity. Consequently, the test wind speed for this experimental investigation is decided to be at 40 m/s, which corresponds to a Reynolds number of 3.7×10^6 .

Reynolds number effect is considered has minimal influence in this kind of testing [4]. Nevertheless, it is necessary to have the same strength of flow field around the main rotor hub devices as if using the long blade. For this, the main rotor rpm is taken so that the blade tip velocity of this short blade would be the same as the one with actual blade length [3]. As the actual main rotor rpm for helicopter's typical operation is about 300 rpm, the main rotor rpm for wind tunnel test must be at 900 rpm, since the short blade is only at one-third of original blade length. By doing this, the same value of Ωr will be maintained.

$$\Omega_{\text{short blade}} = \Omega_{\text{original blade}}$$

where Ω = blade rotation (rpm)
 r = blade radius (m)

3.0 RESULTS AND DISCUSSION

The blade setting angle for this test is -6.5° and the main rotor rotates in counter-clockwise (from top looking upstream) direction. The blade setting angle and rotating direction of main rotor are not an issue here as the blade is assumed not to be the source of wake excitation for tail shake [3]. To confirm this assumption, tests were run with different blade setting angles and opposite direction of main rotor rotation, and the turbulence intensity readings obtained were then compared.

Table 3: Turbulence intensity (%) at point 2, plane B at $V = 40$ m/s

	I	II
Main rotor rotation (0 rpm)	8.664	8.771
Main rotor rotation (900 rpm)	9.354	9.370

where:

Setting I = Blade angle -6.5° , Counter clockwise rotation direction
 Setting II = Blade angle -1.5° , Clockwise rotation direction

Results shown in Table 3 agree with the assumption made. Figure 11 shows the model mounted in UTM-LST's test section.



Figure 11: Model during testing in UTM-LST

3.1 Model at Zero Angle of Attack and Yaw Angles, $V = 40$ m/s

To study how the wake behaves in response to the increasing of main rotor rpm, the main rotor rpm sweep test was conducted from 0 to 900 rpm.

Table 4: Turbulence intensity (%) for plane C

Point	Main Rotor Rotation (rpm)			
	0	300	600	900
1	6.409	6.890	7.451	8.541
2	10.392	11.420	11.25	11.124
3	0.234	0.248	0.300	0.604
4	0.198	0.231	0.223	0.220

From Table 4, it can be concluded that for all points, the minimum turbulence intensity always happens when there is zero main rotor rotation. At Point 1 and 3, the wake increases with main rotor rpm, vice versa for point 2 and 4, the wake is about steady, indicating no influence of main rotor rpm at these two points.

As high wake demonstrated at Point 1 and 2, further investigation was done on these points at Plane B, also at zero angle of attack and yaw angle. This is to study how the wake evolved from Plane C to Plane B.

Table 5: Turbulence intensity (%) for plane B

Point	Main Rotor Rotation (rpm)	
	0	900
1	0.416	1.027
2	8.632	9.354

Compare to Plane C's results, the wake intensity is lower at Plane B as illustrated in Table 5. This is predicted as Plane B is located further downstream.

To further investigate on the contribution of main rotor assembly towards turbulence intensity, the main rotor assembly was taken out. Table 6 obviously tells without the main rotor assembly, the turbulence intensity drops drastically. Hence special attention need to focus on it since reduction of the unsteady wake triggered by it could significantly reduce tail shake.

Table 6: Wake contributors at point 2, plane B

Turbulence Intensity (%)		
No main rotor assembly	With main rotor (0 rpm)	With main rotor (900 rpm)
7.607	8.632	9.354

Table 7 shows some correlation between turbulence intensity and aerodynamic load for configuration with and without main rotor assembly. Both drag coefficient, C_D and turbulence intensity demonstrate the same trend i.e. decrease at configuration with no main rotor assembly. With the main rotor assembly, it increases turbulence intensity to about 19% higher and for the C_D , it leads to about 35% increment. This finding is agree with what had been reported by Philippe et al [4] which cites the hub/pylon combination typically represents between 30 to 40% of the total parasite drag.

Table 7: Correlation with drag coefficient

Configurations	Turb. Intensity (%) (Point 2, Plane B)	CD
No Main Rotor Assembly	7.607	0.0097
Main Rotor (900 rpm)	9.354	0.0149

3.2 Model Undergoing Angle of Attack and Yaw Sweeps (-10° to +10°)

Figure 12 translates the wake behaves non-linear towards angle of attack and yaw sweeps. This is most probably due to rotation of main rotor and unsymmetrical shape of the above part and lower part, as indicated in Figure 13. For angle of attack sweep, it shows higher turbulence intensity occurs at nose down configuration, compared to nose up configuration. This finding tally with what had been reported by NLR report [1].

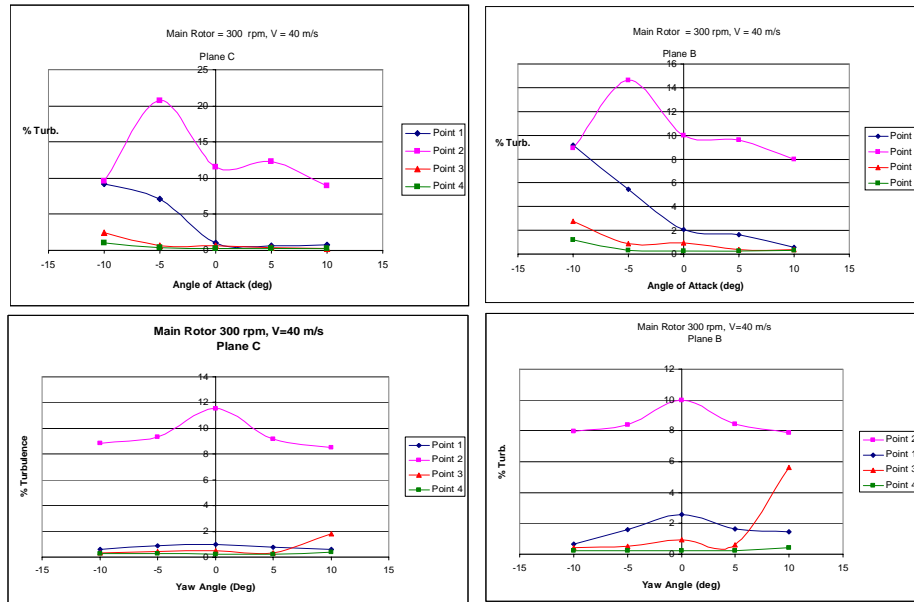


Figure 12: Turbulence intensity characteristics during angle of attack and yaw sweeps

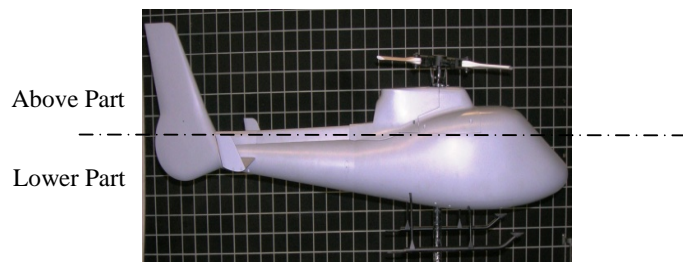


Figure 13: Side plane of the model

Figure 14 depicts the wake characteristics without main rotor rotation. Interestingly, at this location i.e. Point 2 in Plane C, turbulence intensity is about the same at with and without main rotor rotation for zero yaw angle.

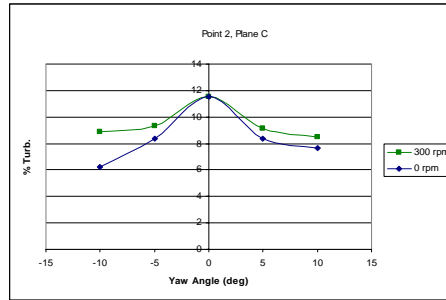


Figure 14: Turbulence intensity at with and without main rotor rotation during yaw sweep

Figure 15 suggests that for the same angle of attack and yaw angles, the wake recedes as it moves further downstream. Figure 16 also shows that the hysteresis of this experiment was really good. For this, the model at first was pitch from angle -10° to 10° , with angle interval of 10° . And then it was repeated again but with opposite sweep angle i.e. started from 10° to -10° .

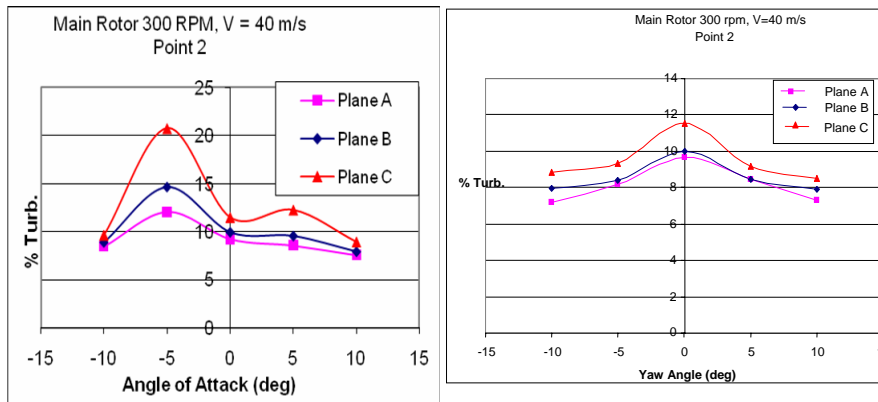


Figure 15: Turbulence intensity at various planes

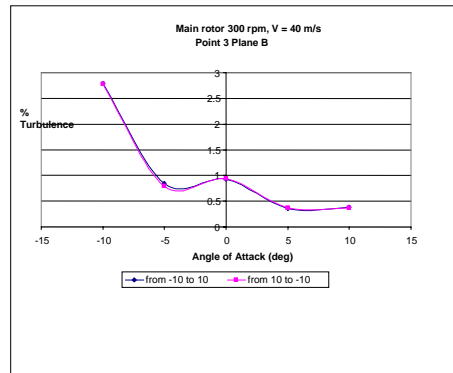


Figure 16: Hysteresis study on angle of attack sweep

Figure 17 depicts turbulence intensity at the most when model is at zero angle of attack and yaw angles at point 2, plane A. Interestingly at this plane, turbulence intensity becomes inversely proportional with main rotor rpm.

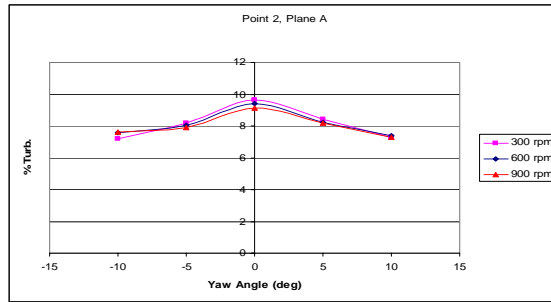


Figure 17: Effects of main rotor rpm sweep during yaw sweep

Undoubtedly, it is also important to investigate on how the wake behaves without the interference of tail part assembly. For this, test were also conducted with a model without the tail part assembly, thus having no horizontal nor vertical tail, as illustrated in Figure 18.



Figure 18: Model without horizontal and vertical tails

Figure 19 depicts how turbulence intensity behaves when there is no tail part assembly. At this specific coordinate i.e. Point 2, Plane B, it seems turbulence intensity becomes lower when there is no tail part assembly.

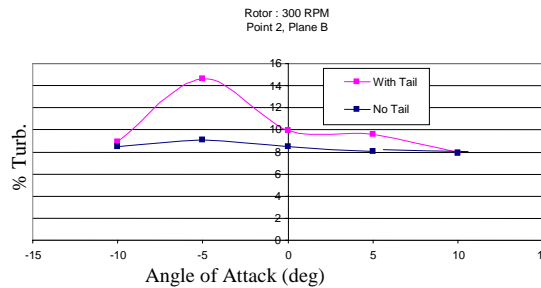


Figure 19: Effects of tail part on turbulence intensity

4.0 CONCLUSION

This paper presented some of the wake characteristics behind the tail part of a generic 350Z Eurocopter helicopter. Some interesting and important findings had been reported e.g. hazardous tail shake likely to happen at during nose down attitude, compared to at nose up attitude of the helicopter. Based on this initial experimental investigation, the most severe wake occurred when the model is nosed down at -5° . Therefore, it is advisable that this model not to fly at this specific angle of attack to avoid vigorous tail shake.

On top of that, results presented in this paper show some correlations between turbulence intensity and aerodynamic load i.e. higher turbulence intensity is likely to contribute to higher aerodynamic drag. This correlation between the unsteadiness and aerodynamic drag is something which could be interesting to be investigated on this helicopter tail shake phenomenon. For future works, further investigation on dynamic analysis should be done for a better understanding of this unsteady aerodynamic wake phenomenon.

REFERENCES

1. Waad, P.G. de and Trouvé, M., 1999. Tail Shake Vibration, NLR, *American Helicopter Society Annual Forum*.
2. Finn, E., 2001. *How to Measure Turbulence with Hot-wire Anemometers*, Dantec Dynamics A/S.
3. Christophe CASTELLIN, 2007–2008. *Email Conversation*. Aerodynamic Department, Eurocopter France.
4. Roesch, P. and Andre, M. Dequin., 1983. Experimental Research On Helicopter Fuselage And Rotor Hub Wake Turbulence, Aerospatiale France, *American Helicopter Society*.